Surface Science 633 (2015) 8–16

Contents lists available at ScienceDirect

Surface Science

journal homepage: www.elsevier.com/locate/susc

Interface of Pt with $SrTiO_3(001)$; A combined theoretical and experimental study

S.E. Stoltz [a,*], D.E. Ellis [b], M.J. Bedzyk [a,b]

[a] Dept. of Materials Science & Engineering, Northwestern University, Evanston, IL 60208, United States
[b] Dept. of Physics & Astronomy, Northwestern University, Evanston, IL 60208, United States

ARTICLE INFO

Article history:
Received 19 July 2014
Accepted 11 November 2014
Available online 15 November 2014

Keywords:
Metal–support interaction
X-ray standing wave
Density Functional Theory

ABSTRACT

Density Functional Theory and X-ray standing wave atomic imaging are combined to develop models of platinum overlayers, patches and small particles on (001) surfaces of $SrTiO_3$. The higher coverage (0.3 ML nominal Pt) experimental result matches best to a simple 1 × 1 surface model. For lower coverage (0.1 ML) a Ti deficient TiO_2 double layer termination is identified as most favorable. A simple model is developed by which XSW amplitudes can be used to infer the aspect ratio of surface structures.

1. Introduction

Heterogeneous catalysts are crucial for numerous large-scale industrial and environmental applications, but the chemical reactions that occur at their surfaces are not yet well understood. Real catalysts, such as metal nanoparticles on porous oxide supports, have complex surfaces, which are difficult to characterize. However, much can be learned using model catalysts that consist of dispersed ad-atoms, nanoparticles, or thin films deposited on a clean, atomically flat support. These surfaces provide a window into the fundamental phenomena governing heterogeneous catalysis.

Oxide supported noble metal nanoparticles show dramatically enhanced catalytic activity compared to defect-free noble metal surfaces due to their rich variety of exposed facets and corners [1–3]. An ideal support would stabilize a nanoparticle catalyst with the desired faces exposed. Such a catalyst could take advantage of the differences in selectivity and reactivity of different faces, which have been found on oriented single crystals [4]. One example is Pt on $SrTiO_3$, a known photocatalyst for water splitting [1], which however suffers from low efficiency. Pt and $SrTiO_3$ (STO) have very similar lattice constants (3.9051 Å for STO and 3.924 Å for Pt), which facilitates cube-on-cube epitaxy *i.e.* Pt(001) || STO(001), Pt[100] || STO[100] [5]. Further studies on optimized Pt_N/perovskite systems could lead to real improvement in performance.

As reported earlier, for physical vapor deposited (PVD) Pt on 2 × 1 STO(001) surfaces annealed to ~900 °C, we produced experimental atomic density maps for the resultant Pt nanoparticles relative to the STO lattice [6]. The 3D density maps are model independent and generated by Fourier inversion with Fourier coefficients obtained by X-ray standing wave (XSW) experiments [7,8]. The Pt atomic density $\rho(\mathbf{r})$ is given by:

$$\rho(\mathbf{r}) = 1 + 2 \sum_{H \neq -H,\, H \neq 0} f_H \cos(2\pi P_H - 2\pi \mathbf{H} \cdot \mathbf{r}) \ , \qquad (1)$$

where $f_{\mathbf{H}}$ is the normalized (0 to 1) Fourier amplitude (or coherent fraction) and $P_{\mathbf{H}}$ is the normalized Fourier phase (or coherent position) obtained from the XSW measurement at each selected $\mathbf{H} = hkl$ substrate Bragg reflection. Based on symmetry, each off-normal Bragg reflection (*e.g.* [011]) has symmetry equivalents (*i.e.*, [0-11], [-101], [101]), which are assigned the same values for $f_{\mathbf{H}}$ and $P_{\mathbf{H}}$ in the summation. Fig. 1 shows the Pt atomic density maps for the two samples of this previous study, where the ultra-high vacuum (UHV) deposition process led to an average Pt coverage of 0.30 monolayer (ML) and 0.1 ML [9]. Atomic-force microscopy indicated the formation of nanoclusters supported on the STO(001) single crystal surface. The XSW 3D Pt atomic maps of Fig. 1 indicate that the nanoclusters are Pt nanocrystals correlated to the underlying STO lattice; each coverage having a distinctive Pt atomic arrangement [6]. In both cases Pt atoms occupy a face-centered-cubic (FCC) lattice, which is in registry with the substrate cubic-P lattice. Further, integration around the Pt positions (high density areas) shows that for the 0.30 ML case the integrated density is about equal for all Pt positions. While for the 0.1 ML the integrated density is lower for the $z = 0.07$ positions than for the $z = 0.57$ positions. Herein, *x, y,* and *z* refer to fractional unit cell coordinates of the underlying substrate lattice constant, with the Sr atom at the origin.

Theory and modeling are needed, in conjunction with atomic-scale measurements to analyze prototypical nanoparticle/substrate interfaces. XSW gives structural data with sub-Å resolution about the

---

[*] Corresponding author.
E-mail address: svenstoltz@hotmail.com (S.E. Stoltz).

http://dx.doi.org/10.1016/j.susc.2014.11.011
0039-6028/

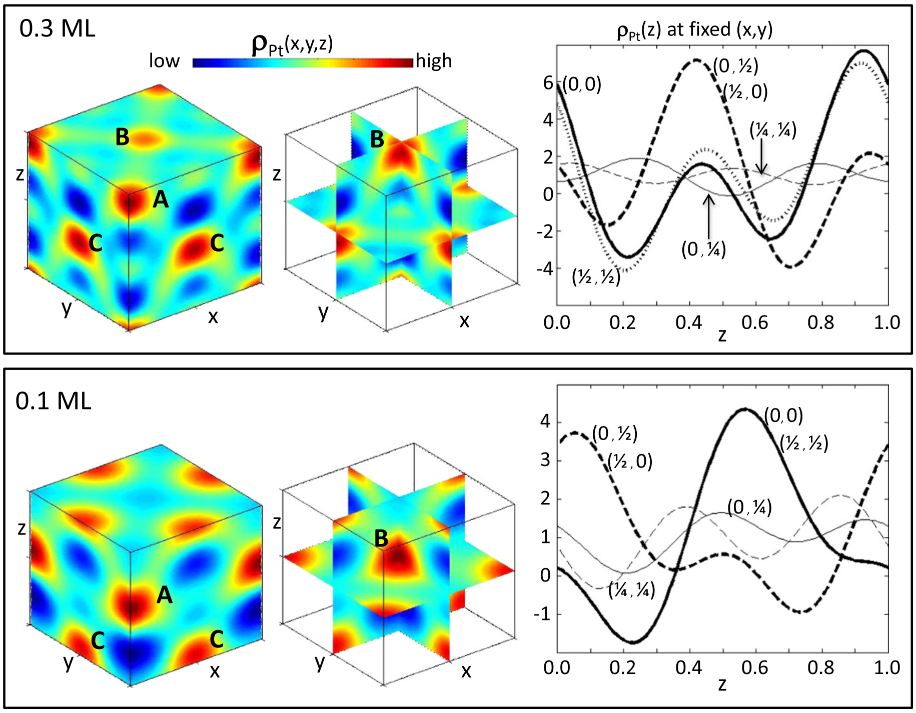

Fig. 1. Left: XSW generated atomic density maps for 0.3 ML (top panel) and 0.1 ML (bottom panel) with respect to the outlined cube of the $SrTiO_3$ bulk unit cell with Sr at (0,0,0). (From Ref. [6].). These maps are model independent and constructed from a summation of XSW measured Fourier components using Eq. (1). The x, y, and z-axes are in the [100], [010], and [001] directions, respectively. Right: Pt atomic density along the z-direction for several high-symmetry (x,y) lateral positions. One notices a slight difference between in Pt atomic density for x,y = 0,0 and ½,½ in the 0.3 ML case. This feature originates from the [011] Fourier component which was only measured for the 0.3 ML case.

position of the Pt atoms with respect to the $SrTiO_3$ bulk unit cell, but no direct structural information about the substrate atoms (O, Ti or Sr) at the interface. However, the extremely high resolution of the XSW technique (<0.1 Å) permits an accurate comparison with Density Functional Theory (DFT) calculated structures. Plausible structural DFT models can be tested against the XSW experimental data, which give detailed atomic scale information for the nanoparticle and support interaction. This is the first work which combines XSW atomic imaging with DFT for a supported nanoparticle system. Examples of other work on this system [10,11] provide very limited comparisons with experiment, and in Ref. [12] where scanning electron microscope images of $SrTiO_3$(001) supported Pt nanoparticles are compared with surface/interface energies for different shapes. Recent TEM work [13] indicates that a clear majority of the Pt clusters grow with cube-on-cube epitaxy on STO. Also note that XSW (as opposed to TEM) gives Pt positions with respect to the STO 3D unit cell that are ensemble averaged over a very large number of Pt clusters. In a recent combined XSW and DFT study [14], WO_x/α-Fe_2O_3(0001) was modeled with DFT and the positions of the W atoms for plausible structures were compared with previously published XSW data. A significant feature of the present work is consideration of Ti- and oxygen-deficient modifications of the oxide–Pt interface, which may occur as a function of coverage, temperature, oxygen pressure and other variables.

2. Computational details

The calculations were performed using the VASP code (Vienna Ab-Initio Simulation Package) with a plane wave basis set [15]. The interactions between ionic core pseudopotentials and valence electrons were modeled using the projected augmented wave method, with a cutoff energy of 400 eV and executed with the generalized gradient exchange–correlation approximation (GGA) as developed by Perdew and Wang [16]. Grids for Brillouin zone integrations were generated automatically by the method of Monkhorst and Pack [17]. We used 6 × 6 × 6 k-point meshes for bulk calculations. Larger meshes, such as 8 × 8 × 8 were found to give no significant difference for the lattice parameter and cohesive energy. For both $SrTiO_3$ and Pt we calculated bulk lattice parameters to be slightly larger than the experimental values, which is typical for GGA and agree well with previous reported values [10,11]. For STO we get 3.94 Å and for Pt 3.99 Å, which should be compared with the X-ray crystallographic values of 3.9051 Å and 3.924 Å, respectively. For STO bulk the Bader charges and atomic volumes were found to be Sr: +1.56e/16.6 $Å^3$, Ti: +2.12e/8.1 $Å^3$, and oxygen: −1.22e/12.2 $Å^3$. Topological Bader charges are defined by zero-flux charge density surfaces about each nucleus [18].

To model surfaces an infinite periodic slab model was mostly used, with the DFT calculated value of $a = 3.94$ Å for x/y cell parameter. Some comparison calculations were also made with the crystallographically determined lattice constant $a = 3.9051$ Å. The dimension of the super-cell was chosen as $a \times a \times c$ (for 1 × 1 surface mesh models) or $2a \times a \times c$ (for 2 × 1 surface meshes); $c = 25$ Å was found to give a sufficient vacuum gap to minimize interslab interactions for all models presented here. For the super-cells 6 × 6 × 4 k-point meshes were chosen for accurate data; less dense meshes such as 5 × 5 × 3 and 4 × 4 × 3 were also found to give adequate precision for comparison between models. Fig. 2 shows a schematic of the surface models used in this work; within the periodic slab the bottom Sr–O layer as well as the first Ti–O_2 layer are held fixed in their bulk positions, while atoms above are allowed to relax. Both single Ti–O_2 and double $(Ti–O_2)_2$ terminations have been studied, guided by numerous experimental studies of STO surfaces [19–21]. The basic slab model adopted for the single Ti–O_2 termination is in total 4 layers thick, with atoms in the top two layers allowed to relax. For the Ti–O_2 double termination another Ti–O_2 layer is added, and here the top 3 layers are relaxed. This highly constrained model was verified previously [22] in extensive studies on Pd–STO interactions, and further tested in the present work by selectively adding one or more layers to the slab. It was verified that using a model slab with more layers does not change the results in any significant way

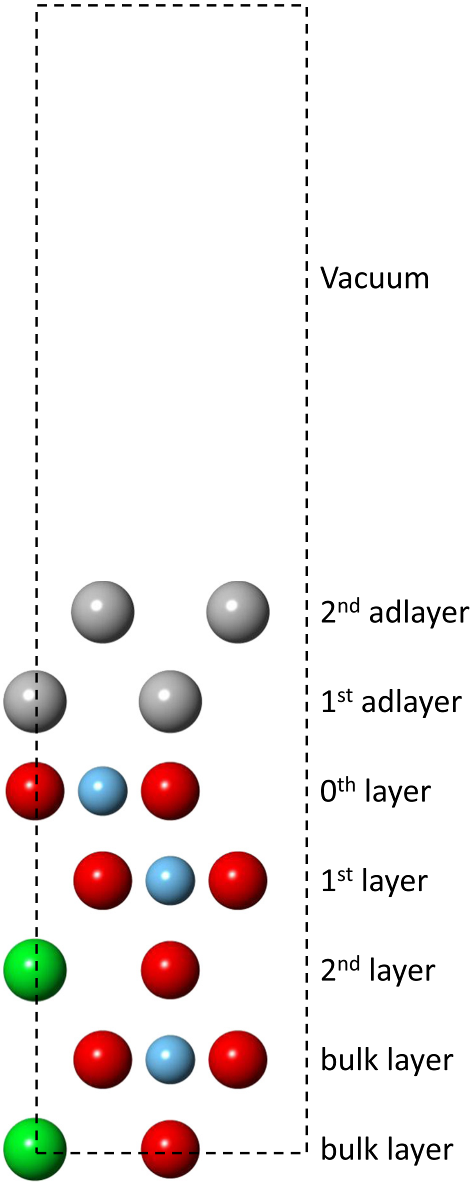

Fig. 2. A schematic of the periodic surface slab used in calculations. In the bottom two layers atoms are held in their bulk positions, while atoms above are allowed to relax. This figure shows the self-consistent relaxed arrangement for 2 ML Pt on a double Ti–O_2 terminated surface with Pt atop O. Color coding of the atomic spheres: gray = Pt, red = O, blue = Ti, and green = Sr. (For interpretation of the references to color in this figure legend, the reader is referred to the web version of this article.)

(*e.g.* changes in atomic positions are <0.02 Å). Initial positions for all calculations were chosen with atoms placed in flat layers separated by $a_{STO}/2$ (in both substrate and Pt ad-layers).

Energies per cell or energies per Pt atom are generally reported in the following with respect to a reference state calculated with the same boundary conditions; *e.g.* the designation "isolated Pt" will refer to a spin-polarized Pt atom in the mid-gap region between STO slabs or in a large periodic box as appropriate. Since we propose in the following that a cation deficient surface is consistent with both low and high Pt coverage XSW data, defect formation energies are also necessary. The vacancy formation energies at Ti and O bulk sites were calculated to be 22.57, 10.16 eV, respectively; different values would apply for ions at and near the crystal surface. With the chosen pseudopotential, the energy of a spin-polarized Pt atom in a 10 × 10 × 10 $Å^3$ cell was found to be −0.635 eV with respect to the non-polarized isolated atomic state. All Pt–STO models were calculated in a spin-restricted format, consistent with diamagnetic Pt–STO interfaces.

3. Results and discussion

3.1. $SrTiO_3$ slabs

First we examine structures of several STO slab models, which serve as a substrate support for the Pt. For the single Ti–O_2 terminated 1 × 1 × 2 slab the two surface oxygen atoms are equivalent and have relaxed positions 0.09 Å higher than the surface Ti atom ($s_1 = 0.09$ Å). Also the distance between the 1st and the 2nd layer is predicted to be 0.13 Å shorter than the bulk value, while the distance between the 2nd and the 3rd layer is 0.11 Å longer (*i.e.* $\Delta d_{12} = -0.13$ Å and $\Delta d_{23} = +0.11$ Å). Average positions in each layer (Fig. 3a) are used in Tables 1 and 2. As described previously, the bottom two atomic layers are fixed at bulk sites. As an example of insensitivity of relaxed structures to frozen atom boundary conditions, addition of a further stoichiometric unit, forming a $1-1-3$ slab and again relaxing all but the bottom two layers was verified to cause changes less than 0.015 Å in position.

Fig. 3b shows a $1-1-2$ double Ti–O_2 terminated model where the top Ti–O_2 layer is displaced a half unit cell in the [100] direction with respect to the layer below. We will refer to this arrangement as double Ti–O_2 terminated. The Ti atom in the termination layer sits atop an oxygen atom, one of the oxygen atoms sits atop Ti, and the other oxygen atom sits atop a hollow site. The oxygen atoms are therefore non-equivalent and their relaxed z-positions differ. The oxygen atom which sits atop hollow, O1, is 0.67 Å higher than the oxygen, O2, which sits atop Ti. The Ti atom in the termination layer has its relaxed height in between (Fig. 3b). By denoting the additional Ti–O_2 layer as the 0th layer we get: $s_0 = 0.67$ Å, $s_1 = 0.28$ Å, $\Delta d_{01} = +0.29$ Å, $\Delta d_{12} = +0.02$ Å and, $\Delta d_{23} = +0.02$ Å.

The best agreement between the experimental results [6] with 0.3 ML Pt coverage (*vide infra*) and various models considered was obtained by using a slab without Ti in the termination (Fig. 3**c**). We will refer to such models as 'Ti-depleted' or 'γ'. When the slab relaxes the oxygen which sits atop a hollow (O1), moves far down. The result is a very open surface termination with one single oxygen atom (O2) per surface unit cell. This isolated slab converges well, but without adsorbed Pt, this surface model is likely only of theoretical interest. It will also be useful to consider an oxygen-depleted modification, '*O-dep*' of the 2 × 1 Ti-displaced double termination in the following.

3.2. $SrTiO_3$ reconstructions

The 2 × 1 reconstruction for the double Ti–O_2 model can be described as a displacement of one of the Ti atoms in the termination layer, while the O atoms remain in their original 1 × 1 positions [19]. The name Ti-displaced, *Ti-disp* (there is only one possibility with Ti atop O), will be used for this 2 × 1 reconstruction. Many other observed superstructures (2 × 2, c(2 × 4), (√2 × √2)R45°, 4 × 1) are also explained by Ti displacements together with O positions being relaxed but not displaced laterally [20]. Since our experimental data [6] only show atop or 4-fold sites for Pt adsorption, O atoms in the termination layer which are not moved (just relaxed) are consistent with this picture. The initial atomic positions for DFT calculations form flat layers (Fig. 4), which are then relaxed. The best agreement between the experimental results [6] with 0.1 ML Pt coverage (*vide infra*) and various models considered was obtained by using a slab with 50% Ti deficiency, *i.e.* Ti_1O_4, in the termination layer. We call this the Ti deficient model 'α' (Fig. 4). In the α model the Ti atom which was moved to create the Ti-displaced 2 × 1 model was removed.

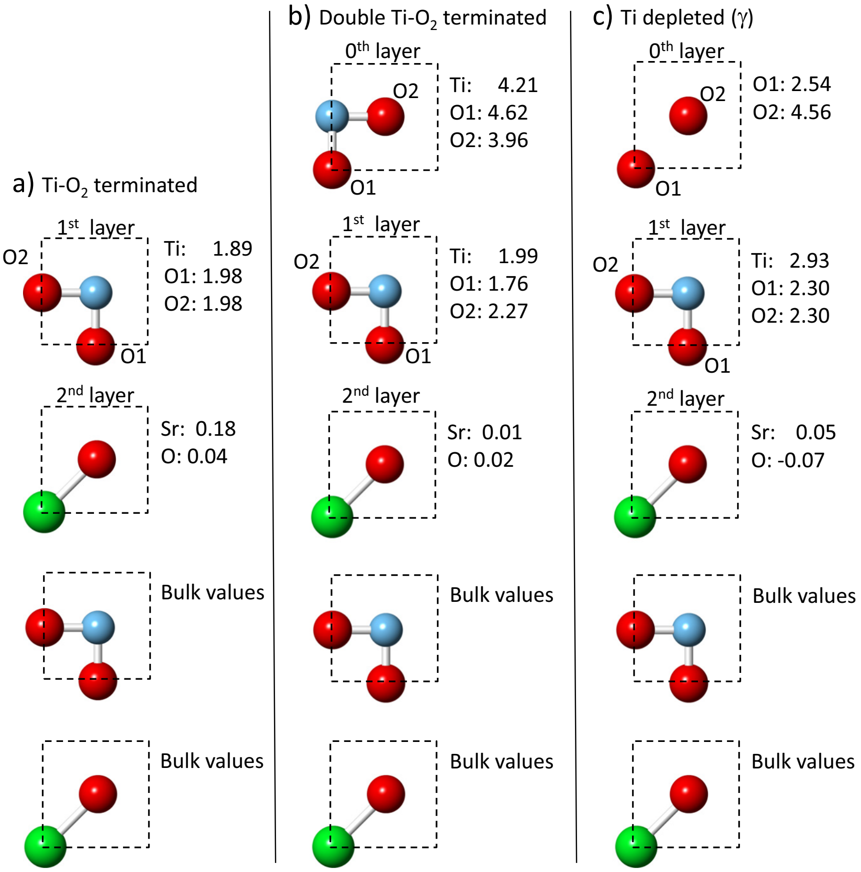

Fig. 3. Slab models with top view of each 1 × 1 layer. The z-positions (Å) of relaxed atoms are shown. The reference position $z = 0$ corresponds to Sr–O bulk planes. (c) O_1 in 0th layer goes down to the 1st layer when the model relaxes.

3.3. Pt adsorption studies

The present study focuses on XSW observed structures [6] which only show atop or 4-fold sites for Pt adsorption, and do not include bridge adsorption sites. Bridge adsorption is observed in TEM studies [13] on Pt:STO nanocubes, in which 61% are found to be cube on cube and 14% are in the bridged R45° structure. The following expression is used for adsorption energy per Pt atom, were N is the number of adsorbed Pt:

$$E_{ads} = \left[\left(E_{slab} + NE_{Pt,gas}\right) - E_{ads-slab}\right]/N. \qquad (2)$$

E_{slab} is the total energy of the relaxed STO slab, $E_{Pt,gas}$ is the energy of an isolated spin-polarized Pt atom (−0.635 eV using a 10 × 10 × 10 $Å^3$ cell; the zero of energy here is the spin-restricted d^9s^1 Pt atom in vacuum) and $E_{ads\text{-}slab}$ is the total energy of the Pt/$SrTiO_3$ slab.

3.3.1. Pt adsorption on unreconstructed (1 × 1) surfaces: ½ ML

For the single Ti–O_2 terminated slab the O-atop (both O atoms are equivalent) site is the most favorable for Pt adsorption; see Fig. 5a. This site has an adsorption energy of 2.46 eV which is about 1 eV more than the O 4-fold hollow and Ti-atop sites which are within 0.02 eV of each other (essentially the same as reported in [10]). The atop Pt – O bond length is 1.99 Å and its z position with respect to Sr bulk is 3.89 Å. Adsorption energies, coordinates and bond lengths for some of the cases studied are compiled in Table 1. Table 2 presents a comparison of Pt positions between the experimental data and more favorable models. Positions are given in fractional coordinates with respect to the STO bulk unit cell with Sr at the origin (0, 0, 0). The ambiguity of XSW positions in terms of integer multiples of the unit cell is thus removed.

For double Ti–O_2 terminated models the O-atop sites are not equivalent, which gives four competing adsorption sites (Fig. 5b). The O1-atop site is most favorable but the binding energy of the hollow site is almost as great (2.79 and 2.63 eV respectively). The Pt – O bond length for the O1-atop adsorption site is 1.95 Å. For the 4-fold hollow case the Pt – O bonds are 2.03, 2.63 Å for O1 and O2 respectively. The Pt z-coordinate is 6.25 Å and 5.66 Å for the O1-atop and 4-fold hollow, respectively. Data for atop-O2 and atop-Ti models can also be found in Table 1.

For the Ti-depleted γ model there are two equivalent 4-fold hollow adsorption sites (Fig. 5**c**) which are clearly most favored, by more than 4 eV. Here the Pt ad-atom appropriates the empty Ti site, and significantly smooths the surface; the difference in z-position between O1 and O2 in the termination layer is reduced from 2.03 Å to 0.6 Å. Further information can be found in Table 1. We may consider that calculated adsorption energies for this system are unphysically high (9.25, 4.91, 4.07 eV) for 4-fold, O2, O1 respectively. Bearing in mind the high bulk Ti vacancy formation energy (22.5 eV) we may suppose that Pt is recovering part of the (missing) cation Coulomb energy. The very open surface (terminated with only one O atom per surface unit cell) for the relaxed γ slab makes further comparisons with ideal structures difficult. However, relative energies between different adsorption sites on this surface are expected to be accurate.

3.3.2. Mono- and multi-layer Pt adsorption on unreconstructed (1 × 1) surfaces

Two Pt atoms placed on either the atop-O sites, or in the 4-fold sites (atop-Ti and 4-fold hollow) correspond to 1 ML Pt coverage for the unreconstructed 1 × 1 surface. For both the single and double Ti–O_2

Table 1
Adsorption energies (eV/Pt), interatomic distances (Å), and z-coordinates (Å) for Pt ad-atoms. Values within parentheses are from Ref. [10]. Bond lengths are given between Pt in the contact layer and atoms in the substrate termination layer. Z_{Pt} is the height of Pt atoms with respect to Sr–O bulk planes, modulo a = 3.94 Å where a single number is given it is the average over similar sites; otherwise a range of values is indicated. Entries in bold are energetically favored states for a given surface/coverage model.

	E [eV]	Pt – O [Å]	Pt – Ti [Å]	z_{Pt} [Å]
1 × TiO_2 terminated				
½ ML				
Atop O	**2.46** (2.47)	1.99 (2.02)	2.76	3.89
Hollow	1.45 (1.51)	2.60 (2.61)	3.26	3.65
Atop Ti	1.43 (1.43)	–	2.49 (2.46)	4.45
1 ML				
Atop O	**3.92** (3.96)	2.21 (2.23)	–	4.13
4-fold	3.90 (3.84)	2.91 (3.38)	2.67, (2.77)	4.08, 4.63 s_{Pt} = 0.55, (0.44)
2 ML				
Atop O	**4.84** (4.87)	2.16	–	4.08, 4.08 6.09, 6.11
4-fold	4.73	3.5	2.99	4.87, 4.91, 6.85, 6.85
2 × TiO_2 terminated				
½ ML				
Atop O1	**2.79**	1.95	>3	6.25
Atop O2	2.11	2.06	–	6.04
Hollow	2.63	2.03, 2.63	>3	5.66
Atop Ti	1.84	2.63	2.36	6.64
1 ML				
Atop O(**½,½**) (0, 0)	**4.15**	1.99	3.03, 3.13	6.61, 6.81
4-fold (**½**,0)(0, **½**)	4.05	2.58	2.57	6.29, 6.86
2 ML				
Atop O	**4.91**	2.05	3.00, 3.15	6.54, 6.74 8.61, 8.65
4-fold	4.75	>3	2.74	6.90, 6.96 8.86, 8.92
Ti-disp atop O	4.75	2.04–2.72	2.92	6.52, 8.53
Ti-disp 4-fold	4.7	2.50–2.66	2.69	6.82, 8.80
2 × TiO_2 Ti-depleted				
½ ML				
γ 4-fold	**9.26**	1.97–2.65	3.26	4.55
γ O2	4.91	1.83	>3	5.75
γ O1	4.08	1.77	>3	4.80
1 ML				
γ atop O (**½,½**)(0,0)	5.59	1.80,1.85	>3	5.92,5.94
γ 4-fold (hollow) (**½**,0)(0, **½**)	**6.04**	2.01, 2.29	>3	5.29
1.5 ML				
γ atop O	5.37	1.72, 1.88	–	5.93, 5.91 7.75
γ atop O, Pt as cation	5.97	1.93–2.31	3.15	4.42 6.72, 7.06
α atop Ti	5.77	1.99–2.19		5.05–7.08 7.65–8.78
α atop O	**6.07**	1.80–2.08	2.86	6.03–6.35 7.92–7.96
β atop O	4.93	1.85–1.95	3.24	6.15–7.61 7.99, 8.60
2 ML				
γ 4-fold (hollow)	**5.45**	2.18, 2.32	–	5.40, 5.40 7.47, 7.34

Table 2
Comparison of Pt positions obtained from experiment (Fig. 1) and calculated with DFT. The table shows the fractional z-coordinate of Pt with respect to the $SrTiO_3$ bulk unit cell, where we define the Sr atom to be in the (0,0,0) position. A *sign indicates that the Pt atom on this position is part of the contact layer. The best representative DFT model for the 0.30 ML experimental case is 2 ML of Pt on a 1 × 1 O_2-γ surface. For the 0.1 ML case we found that a DFT model with 1.5 ML of Pt on 2 × 1 Ti_1O_4-α surface works best. For XSW a_{STO} = 3.9051 Å for DFT a_{STO} = 3.94 Å if not stated different.

Lateral high-symmetry site	A-site	B-site	C-site	C-site
(x,y) coordinate of site	(0,0)	(½,½)	(½,0)	(0, ½)
XSW experimental:				
0.3 ML model independent	0.92	0.90	0.40	0.40
0.1 ML model independent	0.57*	0.57*	1.07	1.07
0.3 ML model dependent	0.97	0.91	0.41	0.41
0.1 ML model dependent	0.60	0.61	0.91	0.91
DFT 1 × 1 surfaces 2 ML:				
Ti–O_2 terminated Pt atop Ox	0.55	0.54	0.04*	0.04*
Ti–O_2 terminated Pt 4-fold	0.24*	0.25*	0.74	0.74
Double Ti–O_2 terminated Pt atop Ox	0.66*	0.71*	0.19	0.20
Double Ti–O_2 terminated Pt 4-fold	0.25	0.27	0.75*	0.77*
O_2-γ model Pt atop Ox	NaN	NaN	NaN	NaN
O_2-γ model Pt 4-fold	0.90	0.86	0.37*	0.37*
O_2-γ model Pt 4-fold (a = 3.905 Å)	0.92	0.89	0.39*	0.39*
DFT 1 × 1 surfaces 1.5 ML				
O_2-γ model Pt atop Ox	0.51*	0.50*	Empty	0.97
O_2-γ model Pt atop Ox (cation case)	0.71	0.79	Empty	1.12
DFT 2 × 1 surfaces:				
Ti_1O_4 α 1.5 ML Pt atop Ox	~0.56*	~0.56*	~1.01	~1.01
Ti_1O_4 α 1.5 ML Pt atop Ox (a = 3.905 Å)	~0.59*	~0.59*	~1.06	~1.06

terminated slab the adsorption energies were found to be rather similar. Broken down as adsorption energy per Pt atom according to Eq. (2), O-atop is favored by 0.02 eV in the single Ti–O_2 terminated model and by 0.1 eV in the double Ti–O_2 terminated case. On the γ slab the 4-fold site is preferred by 0.45 eV per Pt ad-atom for 1 ML coverage. For 2 ML coverage the atop-O sites are preferred in both the single and double Ti–O_2 terminated slabs although with a rather small energy difference: 0.10 eV for the single Ti–O_2 termination and 0.16 eV for double Ti–O_2 termination. Since the adsorption energy is stated per Pt ad-atom the difference in total energy which favors the O-atop arrangement is 0.42 eV and 0.63 eV per cell, respectively. None of these models however matches the experimental 'high coverage' XSW data. A summary of adsorption energies and structural data for the 1 ML, 1.5 ML and 2 ML coverages can be found in Table 1.

For the γ model the 2 ML coverage stacked in the 4-fold Pt position (Fig. 6a) converges well, while the "atop-O" construction does not. The z-positions for the Pt ad-atoms with respect to Sr bulk for the 2 ML / 4-fold case are: 5.40, 5.40, 7.47 and, 7.34 Å, which are very close to experimental values gathered from the XSW density maps for the high coverage case where maxima where found for z values of 5.46, 5.46, 7.49 and, 7.41 Å (with corresponding x, y values). No other models that were tried give a close match to the high coverage (0.3 ML) experimental data. Using the spectroscopic lattice parameter of $SrTiO_3$ (3.9051 Å) instead of the bulk relaxed value (3.94 Å) gives 0.03–0.06 Å larger values for the Pt z-coordinate; *i.e.* 5.43 Å, 5.43 Å, 7.51 Å and, 7.40 Å which is surely an accidentally close match to experiment. In the present work most DFT calculations were made with the bulk relaxed 3.94 Å lattice parameter. The small differences in results from using 3.9051 Å *vs* 3.94 Å do not alter our conclusions in any way. Table 2 compares Pt positions from XSW experiments with the different DFT models.

3.3.3. Pt adsorption on reconstructed (2 × 1) surfaces

While the Pt positions obtained from the XSW experiment with 0.3 ML nominal Pt coverage could be adequately explained with a 1 × 1 surface model, the same is not true for the lower-coverage 0.1 ML case. It is worth recalling here that only a fraction of the deposited Pt is found by the XSW measurements to be coherent to the STO lattice; results from Ref. [6] show that $c_A + c_B + 2c_C = 0.49$. Normally for a highly perfect single-crystal substrate, such as Si or Ge, this would mean that only 49% of the Pt atoms are correlated with the substrate lattice. However, this is not a perfect single-crystal substrate, as the diffuse tails of the measured reflectivity indicate (Fig. 2 of Ref. [6]). Using XSW analysis of the Ti sublattice within bulk STO(001) as a reference, it was determined that 78% is a better estimate of Pt correlation fraction for the higher coverage case and 40–50% for the lower coverage case. How the coherent patches may be distributed over the STO surface is unknown. A strong Pt – O bonding interaction would favor formation of rafts or islands over Pt_N particles. A 2 ML Pt model on single-TiO_2

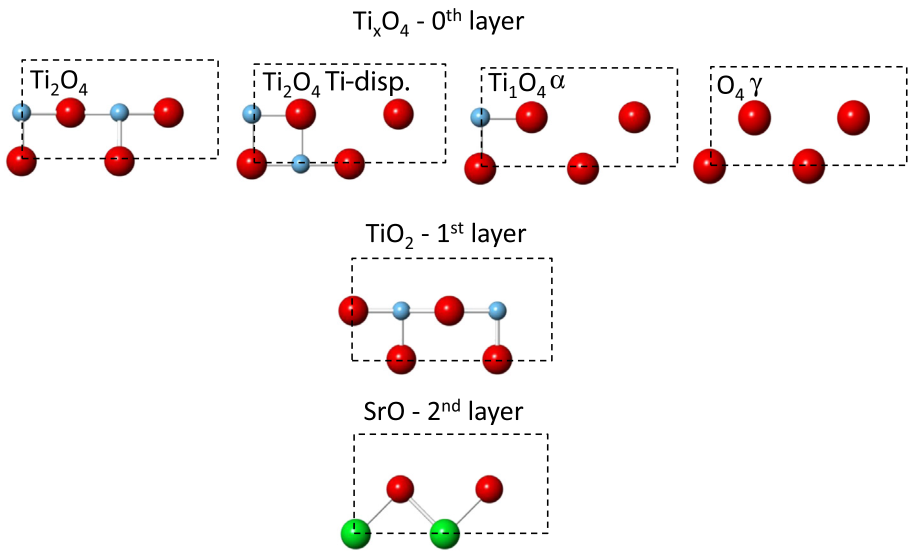

Fig. 4. Top view of top 3 layers for 1 × 2 unit cells for various Ti_xO_4 double-layer terminations.

termination yields Pt positions that match the XSW coordinates: however, the result must be considered unphysical since the contact layer (1st ad-layer) would then correspond to the weaker peaks from the XSW experiment. This would imply that there are fewer Pt atoms in the 1st ad-layer than in the 2nd layer. A similar reasoning applies if extended to more Pt layers.

Ti deficient (Ti-*def*) models with modified Pt coverage resolve this difficulty: here the amount of Ti in the termination layer has been reduced by ½, *i.e.* the Ti atom which is displaced in the *Ti-disp* reconstructed 2 × 1 structure (compared to 1 × 1) has now been removed. Furthermore, the Pt coverage found in the best model is 1.5 ML (*i.e.* 4 Pt atoms in the contact layer and 2 Pt in the 2nd ad-layer). This scheme is supported by XSW results; *e.g.* the density spots in the 3D images which correspond to Pt atoms in the 2nd ad-layer are weaker and can be clearly seen in the $f_{001} > 0$ reflections.

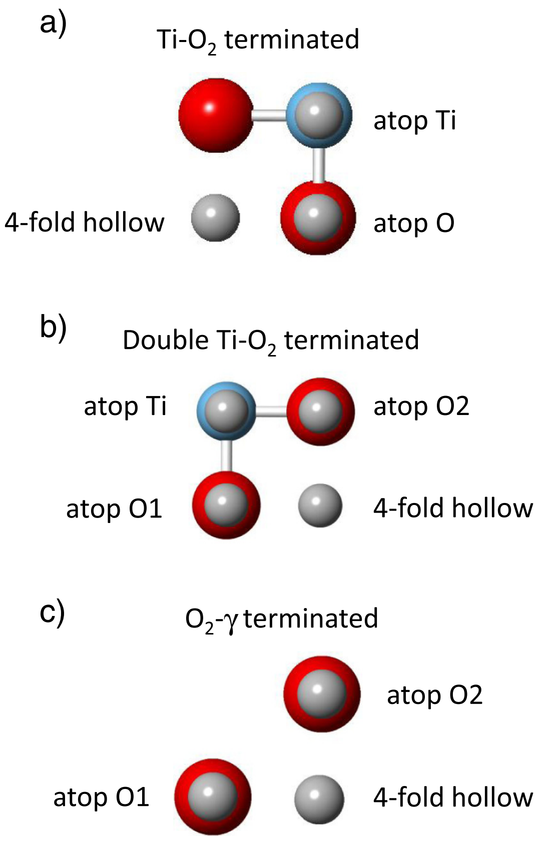

Fig. 5. Top view showing symmetry in-equivalent Pt adsorption sites at Pt/STO interface for the various 1 × 1 STO termination models.

The Ti-*def* configuration labeled α (Ti at x,y = 0, 1/2) with Pt atop O and adsorption energy 6.07 eV/Pt gives best agreement with experiment (Fig. 4). A fairly smooth Pd contact layer is formed (R_{Pt-O}: 1.80–2.07 Å) with a Pt 'dimer' (R_{Pt-Pt} 2.67 Å) forming the overlayer. The z-coordinates are 6.02–6.35 and 7.92–7.95 Å for 1st and 2nd ad-layers respectively for the $a_{STO} = 3.94$ Å model. For the $a_{STO} = 3.9051$ Å model the z-coordinates move slightly upwards to 6.09–6.42 and 8.02–8.04 Å. An interface with contact layer Pt in 4-fold symmetry, *i.e.* 3 Pt atoms in 4-fold hollow and 1 Pt atop Ti is less favored by 0.30 eV/Pt. For the remaining Ti-*def* configuration, β (Ti at x,y = 1/4, 0), there is no satisfactory agreement between 1.5 ML DFT and XSW structural models. Not surprisingly, the Ti site occupancy plays a crucial role in determining Pt adsorption geometry; the complex energy landscape probably permits additional adatom configurations

3.3.4. Additional models

Additional models, more distant from the presumed favorite 2 × 1 double $Ti–O_2$ structures, which have been tested include a Sr–O termination layer and a Ti-depleted single terminated $Ti–O_2$ model. The latter can be considered to be a modification to a model proposed by Castell [21]. In both cases Pt atoms were placed in a 4-fold hollow. None of these models, however, gave relaxed positions of Pt which agree adequately with XSW data.

Higher coverage 2 ML α Ti-*def* structures prove to be consistent with the 1.5 ML results: the atop O and 4-fold atop Ti configurations having energy of 5.93 and 5.76 eV/Pt, respectively. Higher coverage was also investigated in a model which can be described as double $Ti–O_2$ with a single O vacancy, *i.e.*, *O-dep*. For both 2 ML and 2.5 ML Pt coverage an O atop configuration was favored by 0.14 eV/Pt over Ti atop. The topmost atoms in 2.5 ML are rather well isolated from the substrate, and provide an additional binding energy of 5.37 eV/Pt which may be considered a fairly typical value for accretion onto a nucleated surface-bound Pt particle. Pt_N particle models with N = 5, 10, 13, and 20 were further considered to verify stability of structures previously seen in experiment and modeled for Pd_N:STO. As with Pd_N the energy per Pt atom is seen to be a monotonic function of particle size, indicating the

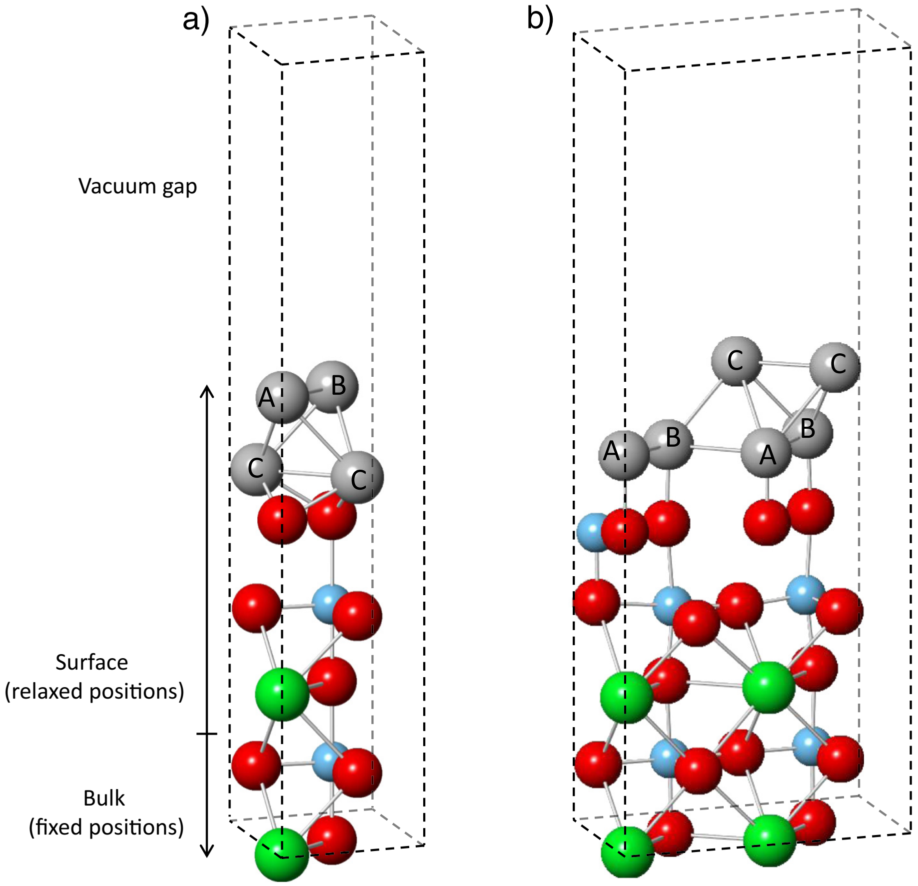

Fig. 6. Models which best fit experiment: (a) 2 ML of Pt on 1 × 1 O_2-γ surface; (b) 1.5 ML of Pt on 1 × 2 Ti_1O_4-α surface. The A, B, and C labels in (a) and (b) correspond to the same Pt site assignments as in Fig. 1 top left and bottom left, respectively.

stability of Pt_N nanostructures on STO, consistent with the experimental observation of particle growth under cyclic oxidation and annealing processes. Those results will be presented elsewhere in conjunction with chemisorption studies.

3.4. Direct comparison with XSW experiment

By the above comparison of the Pt positions from XSW measured Pt atomic density maps (Fig. 1) to the DFT calculated models, we found that the higher coverage data can be best explained with clusters having 2 ML of Pt in the γ model (Fig. 6a). The lower coverage data can best be explained with 1.5 ML Pt on the α model (Fig. 6b). An alternative comparison method is shown in Table 3 where the XSW measured Fourier amplitudes (f_H) and phases (P_H) are compared respectively to the amplitudes, $|A_H|$, and phases, $Arg[A_H]/(2\pi)$, of the normalized Fourier coefficients (or geometrical structure factors), $A_{\boldsymbol{H}}$, calculated from the DFT predicted Pt coordinates, $\boldsymbol{r}_n$, and occupation fractions, c_n (*i.e.* $1/N$, where N is the number of Pt atoms in the model).

$$A_{\boldsymbol{H}} = \sum_{n=1}^{N} c_n \, e^{2\pi i \boldsymbol{H}\cdot\boldsymbol{r}_n}. \tag{3}$$

While the XSW measured and model-calculated phases can be compared directly, the XSW amplitude, f_H, should be compared to the product $C|A_H|D_H$, where C is the correlated fraction of Pt atoms and $D_H = exp(-2(\pi\sigma/d_{\boldsymbol{H}})^2)$ is the Debye–Waller factor that treats the time-averaged and ensemble-averaged displacement field of Pt about the ideal *FCC* sites as an isotropic Gaussian distribution with width σ as compared to the d-spacing $d_{\boldsymbol{H}}$. From the earlier report for the 0.3 ML case [6] one finds $C = 0.49$ ($C = 0.39$ *for the 0.1 ML case*), corresponding to 49% of the Pt being in registry with the STO lattice, and $\sigma = 0.26$ Å. For a RT thermal vibrational amplitude of 0.1 Å the contribution from static disorder would correspond to an amplitude of 0.24 Å. Table 3 also lists f_H and P_H values determined from a global fit described in the earlier study [6], where the same value of σ is used. It is found that the Fourier modified amplitudes and phases generated by the DFT derived geometrical structure factors agree with the experimental data almost as well as the global fit, which represents the best possible agreement. The global

Table 3
Direct comparion between DFT models and XSW experiments: The table shows a summary of Fourier amplitudes, $f_{\boldsymbol{H}}$, and phases, $P_{\boldsymbol{H}}$, from XSW experiment compared with geometrical structure factor (Eq. (3)) using Pt coordinates obtained by DFT (a_{STO} = 3.9051 Å). Results from the global fit of Ref. [6] are shown as well.

0.3 ML	XSW experiment		DFT γ model		Global-fit	
hkl	$f_{\boldsymbol{H}}$	$P_{\boldsymbol{H}}$	$f_{\boldsymbol{H}}$	$P_{\boldsymbol{H}}$	$f_{\boldsymbol{H}}$	$P_{\boldsymbol{H}}$
001	0.07(3)	–	0.03	0.15	0.07	0.07
002	0.39(3)	−0.18(2)	0.34	−0.20	0.32	−0.15
011	0.07(3)	–	0.02	0.15	0.06	0.07
022	0.22(3)	−0.16(2)	0.24	−0.20	0.23	−0.15
111	0.35(3)	−0.13(2)	0.38	−0.10	0.37	−0.07
222	0.15(3)	−0.08(5)	0.17	−0.20	0.16	−0.15
0.1 ML	XSW experiment		DFT α model		Global-fit	
hkl	$f_{\boldsymbol{H}}$	$P_{\boldsymbol{H}}$	$f_{\boldsymbol{H}}$	$P_{\boldsymbol{H}}$	$f_{\boldsymbol{H}}$	$P_{\boldsymbol{H}}$
001	0.21(3)	−0.32(3)	0.12	−0.38	0.25	−0.33
002	0.26(3)	−0.03(3)	0.25	0.15	0.20	0.13
022	0.11(3)	0.15(4)	0.18	0.15	0.20	0.13
111	0.26(3)	−0.39(3)	0.28	−0.43	0.33	−0.45

fit also had a larger parameter freedom since the occupancy fractions (c_n) were not forced to be $1/N$ and the Pt coordinates, ($\boldsymbol{r}_n$) did not have to be relaxed positions.

At this point it is useful to consider what Eq. (3) would predict for an idealized distribution, where Pt atoms only occupy *FCC* sites that are correlated to the STO cubic unit cell. For unmixed (all odd or all even) *hkl* reflections (*e.g.*, (*002*), (*111*)) the complex-plane vectors for the $N = 4$ sites within the Eq. (3) summation will all have the same phase. For mixed *hkl* reflections *(e.g., (001))* the summation will have a pair of Pt site complex vectors perfectly in-phase with each other and perfectly out-of-phase with the other pair of Pt site vectors. Therefore the normalized Fourier amplitude for this ideal Pt atomic distribution would be very close to unity for the unmixed *hkl* reflections. For mixed *hkl* reflections the Fourier amplitude *would be zero*, if all *FCC* sites were equally occupied. However, for Pt nanostructures averaging only a few atomic layers in height, there is a likelihood that each successive layer is significantly less occupied, which would lead to $f_{001} > 0$. The Fourier phase for unmixed *hkl* would be identical to the phase of each term in the summation. For mixed *hkl* with $f_{\boldsymbol{H}} > 0$ the phase will be equal to the phase of the most dominant term in the summation. In such a case, P_{001} would be expected to correspond to the position of the bottom layer in the Pt cluster, if the cluster is "bottom heavy". More specifically, for a geometric progression stacking of M atomic layers where $c_{n+1} = \beta\, c_n$, the *00L* Fourier amplitude would be:

$$|A_{00L}| = \frac{1-\beta}{1-\beta^M}\;\frac{1-\beta^M(-1)^{LM}}{1-(-1)^L\beta}\,. \tag{4}$$

This expression simplifies *to* $|A_{00L}| = 1$ *for even values of L. For odd values of L it simplifies to* $|A_{00L}| = (1-\beta)\,/\,(1+\beta)$ *if M is even or large.* By comparing the ratio $f_{001}\,/\,f_{002}$ one may estimate that $\beta = 0.23(8)$ for the 0.1 ML experiment and $\beta = 0.76(9)$ for the 0.3 ML experiment. This is based on $(f_{001}/f_{002})\, D^3_{001} = (1-\beta)\,/\,(1+\beta)$. Here the factor $D_{002}/\,D_{001} = D^3_{001} = 0.77$ comes from compensation of the Debye–Waller factor, introduced above. This further supports the idea of a tapered DFT model to explain the 0.1 ML data and the non-tapered DFT model for the 0.3 ML case.

For the 0.1 ML case the global fit [6] predicted that there are twice as many Pt atoms in the layer containing the A and B sites (see Fig. 1.) as in the adjacent layer containing the C site which gives a β value of 0.5. This was the main motivation to choose a model with 1.5 ML Pt local coverage to explain the low coverage data. The (001) normalized geometrical structure factor gives a coherent fraction of 0.12 (Table 3) using the previously mentioned 1.5 ML Pt atop O in the α model. If one calculates β using f_{001} and f_{002} for the 2 ML γ model (Fig. 6a) and for the 1.5 ML α model (Fig. 6b) one finds $\beta = 0.88$ and 0.48, respectively. The deviation from actual $\beta = 1$ and ½ originates from the fact that the relaxed position of the Pt in these DFT models deviates from perfectly flat layers separated with $a_{STO}/2$.

The XSW measured coherent fractions (Table 3) for the unmixed *hkl* reflections, (*002*), (*022*), (*111*) and (*222*), being 0.39, 0.22, 0.35, and 0.15 for the higher coverage experiment, and 0.26, 0.11 and 0.26 ((*222*) not measured) for the lower coverage experiment indicate that there is a sizable fraction of uncorrelated Pt. For the mixed *hkl* reflections (*e.g.*, (001)) the picture is slightly more complex. One can therefore divide into higher coverage and lower coverage cases: For the higher coverage case both the experiment and the DFT-based geometrical structure factor give coherent fractions of less than 0.1 for both (*001*) and (*011*). For the low coverage case however the coherent fraction in the (001) reflection was measured as 0.21 (the (*011*) reflection was not measured), which is a clear indication of different number of Pt atoms in each layer, *i.e.* the c_n values in Eq. (3) are not all equivalent.

3.5. XSW observed structural changes during annealing process

In addition to the 3D atomic imaging described above, remarkable structural changes were observed during the step-by-step annealing process under ultra-high vacuum (UHV) conditions that ended at ~900 °C. After each increased temperature step the sample was cooled down to RT for a (002) XSW measurement. Fig. 7 shows the temperature-dependent XSW data for both samples during this annealing process. Between 700 and 800 °C the coherent fraction of the higher coverage sample decreases simultaneously as the coherent position changes, which indicates a significant rearrangement of Pt atoms. Additional annealing to 910 °C increased the coherent fraction while the coherent position did not change. Finally the samples were removed from the UHV chamber to do the more extensive set of XSW measurement in open air to produce the 3D image shown in Fig. 1. For the higher coverage sample P_{002} was unchanged, indicating that the Pt/STO interface remained the same after being exposed to air.

It is difficult to assign any model which explains the Pt atomic position after the anneals of the higher coverage sample to 500 and 700 °C, since only the (002) reflection data are available. One can however conclude that the rearrangement between 700 and 800 °C either involves a large displacement downwards (solid line in Fig. 7) of ~1.6 Å, or a small displacement upwards (since $P_{\boldsymbol{H}}$ is defined as modulo-1 parameter) of ~0.4 Å. Feasible explanations would be that the contact layer in the γ model is created either by: (i) Ti atoms in the double Ti–O termination are pushed into the bulk during annealing, while the Pt atoms sink down in the 4-fold hollow position. Or, (ii) Starting with a single Ti–O terminated interface, O atoms diffuse from the bulk to the interface during the annealing creating an O-only contact layer.

4. Conclusion

XSW data for 'low' and 'high' coverage Pt adsorption on STO(001) show two different structures which evolve under thermal annealing. DFT calculations on a variety of Pt/STO interfaces and overlayer schemes provide plausible structures which fit experiment well. Sub-, mono- and multi-layer Pt upon ideal and reconstructed STO terminations, with and without cation- and anion-depletion, was considered in order to access a considerable range of possible chemical and structural modifications

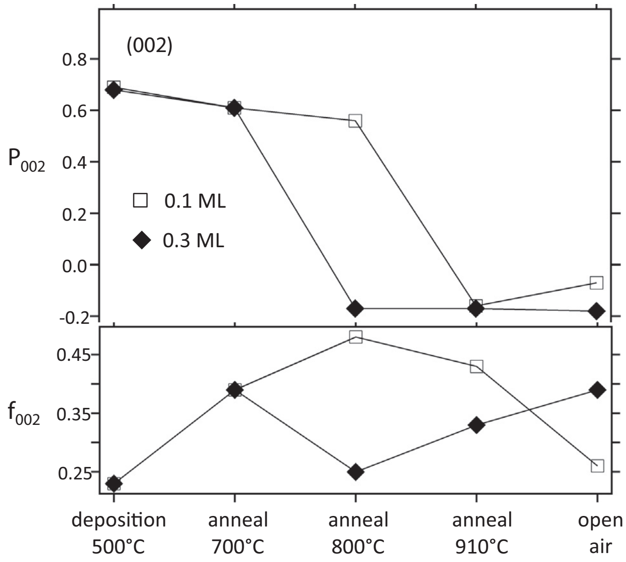

Fig. 7. Temperature dependent XSW data using the STO (002) reflection. The open squares refer to the 0.1 ML experiment and the filled squares refer to the 0.3 ML experiment. Note: since phase P_{002} is a modulo-1 parameter the diagram can also be drawn as P_{002} changing from 0.6 to −0.2 or 0.6 to 0.8 or −0.4 to −0.2. P_{002} can be thought of as the fractional 002 d-spacing displacement of the Pt planes relative to the bulk-like STO planes.

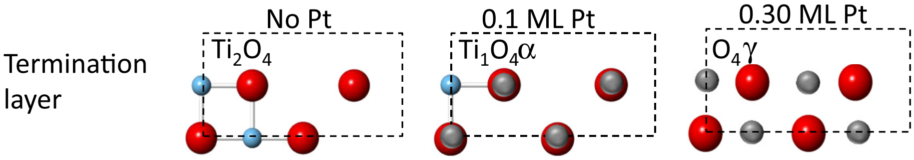

Fig. 8. Top view of 1 × 2 unit cells showing termination layer of $SrTiO_3$ slab in 1 × 1 and 1 × 2 models, and contact layer of Pt. (a) Clean 1 × 2 termination, (b) low coverage 1 × 2 Ti_1O_4-α surface with 1.5 ML Pt atop O, and (c) high coverage 1 × 1 O_4-γ surface with 2 ML Pt in 4-fold hollow site.

to an ‘ideal’ interface. Since experimentally confirmed superstructure models [19,21] require transport of O and Ti between bulk and surface, it is not surprising that adsorbed Pt can modify/select interfacial atomic composition.

A scenario consistent with experiment starts with a 2 × 1 Ti-displaced double $Ti–O_2$ termination which evolves to a Ti-deficient state under annealing in the presence of Pt. For low Pt coverage one of the Ti atoms (the one which was displaced) in the double layer goes into bulk and Pt ad-atoms sit atop O on a termination layer which consists of 1 Ti and 4 O per 2 × 1 cell. This is a metastable transition state. XSW data clearly show two Pt layers, with lower occupancy for the top-most. A 1.5 ML coverage DFT model (Fig. 6b) is found to adequately represent the height and occupancy data. For high Pt coverage all Ti in the termination layer go into the bulk and Pt moves to 4-fold hollow sites (Fig. 6a). This is a stable final state which can be described with a minimal 1 × 1 surface unit cell. In Fig. 8 the interface of between the termination layer of $SrTiO_3$ slab in 1 × 1 and 1 × 2 models, and contact layer of Pt are shown. Both structures facilitate cube-on-cube epitaxy *i.e.* Pt(001) || STO(001) and Pt[100] || STO[100] which is consistent with pyramidal Pt clusters [12].

The temperature dependence of the (*002*) XSW results for the high coverage case suggests Pt on top of a double $Ti–O_2$ layer with all Ti still present up to 700 °C and with a transition to the γ model after the high temperature anneal. This is consistent with the idea that Pt and the high annealing temperature of 900 °C can push Ti into bulk. The final state can also be reached by an alternative model starting with a single $Ti–O_2$ termination layer, followed by oxygen migration to the interface during anneal, thus raising the average Pt height to its equilibrium configuration. The 2 ML Pt with 4-fold coordination on both double and single $Ti–O_2$ termination has $P_{002} = 0.5$ which is reasonably close to 0.6 at 700 °C from Fig. 7.

It is of course possible to continue to build up additional monolayers of Pt. It was (not surprisingly) found that Pt atoms prefer to stack in a face-centered-cubic lattice. However, since the XSW imaging gives the positions of Pt atoms with respect to the STO substrate unit cell, Pt atoms in the 1st and 3rd ad-layer will be mapped on top of each other in the atomic density maps. The DFT calculations give a relative displacement of <0.2 Å for these additional layers compared to the bulk lattice. For the γ model Pt atoms in the 3rd ad-layer will be mapped 0.15 Å higher than Pt atoms in the 1st ad-layer, *i.e.* less than the resolution of the XSW atomic imaging. However, a simple model using the occupation fraction ratio β from layer n to $n + 1$ as a parameter permits further interpretation of A_{00L} amplitudes. A fit of β to experimental data constitutes a measure of the ‘aspect ratio’ of the Pt superstructure. The present data suggests that further exploration of the model in fitting high quality XSW data would be useful.

Acknowledgments

This work was supported in part by the Chemical Sciences, Geosciences, and Biosciences Division, Office of Basic Energy Sciences, Office of Science, U.S. Department of Energy, Grant No. DE-FG0203ER15457, at the Institute for Catalysis in Energy Processes at Northwestern University. Use of the APS at Argonne National Laboratory was supported by the DOE-BES under Contract No. W-31-109-ENG-38. The authors are thankful for discussion and technical assistance from Alexander Kazimirov and Zhenxing Feng.

Appendix A. Supplementary data

Supplementary data to this article can be found online at http://dx.doi.org/10.1016/j.susc.2014.11.011.

References

[1] R.G. Carr, G.A. Somorjai, Nature 290 (1981) 576.
[2] S. Ikeda, K. Hirao, S. Ishino, M. Matsumura, B. Ohtani, Catal. Today 117 (2006) 343.
[3] O. Rosseler, M.V. Shankar, M.K.L. Du, L. Schmidlin, N. Keller, V. Keller, J. Catal. 269 (2010) 179.
[4] T. Hikita, T. Hanada, M. Kudo, M. Kawai, Surf. Sci. 287 (1993) 377.
[5] A.D. Polli, T. Wagner, T. Gemming, M. Ruhle, Surf. Sci. 448 (2000) 279.
[6] Z. Feng, A. Kazimirov, M.J. Bedzyk, ACS Nano 5 (2011) 9755 (ibid, supplementary material).
[7] L. Cheng, P. Fenter, M.J. Bedzyk, N.C. Sturchio, Phys. Rev. Lett. 90 (2003) 255503.
[8] J.S. Okasinski, C.-Y. Kim, D.A. Walko, M.J. Bedzyk, Phys. Rev. B 69 (2004) 041401 (R).
[9] In Ref. [6] a surface coverage of 1 ML was defined as 1 atom per surface STO(001) 1 × 1 unit cell or 6.56 atoms/nm^2. In this work the definition of 1 ML is changed to be 2 Pt atoms per STO 1 × 1 surface unit cell because this corresponds to the maximum density of Pt atoms filling a square lattice defined by the STO 1 × 1 surface unit cell. Therefore the Ref. [5] reported values of 0.60 and 0.17 ML now become 0.3 and 0.1 ML, respectively. Note that the XRF measured coverage is averaged over the mm^2 illuminated surface area and does not sense the coverage heterogeneities due to nano-cluster formation.
[10] A. Asthagiri, D.S. Sholl, J. Chem. Phys. 116 (2002) 9914.
[11] A. Asthagiri, D.S. Sholl, Surf. Sci. 581 (2005) 66.
[12] H. Iddir, V. Komanicky, S. Ogut, H. You, P. Zapol, J. Phys. Chem. C 111 (2007) 14782.
[13] J.A. Enterkin, R.M. Kennedy, J. Lu, J.W. Elam, R.E. Cook, L.D. Marks, P.C. Stair, C.L. Marshall, K.R. Poeppelmeier, Top. Catal. 56 (2013) 1829.
[14] M.E. McBriarty, M.J. Bedzyk, D.E. Ellis, Surf. Sci. 606 (2012) 1367.
[15] G. Kresse, J. Furthmuller, Phys. Rev. B 54 (1996) 11169.
[16] J. Perdew, Y. Wang, Phys. Rev. B 45 (1992) 13244.
[17] H.J. Monkhorst, J.D. Pack, Phys. Rev. B 13 (1976) 5188.
[18] R.F.W. Bader, Atoms in Molecules—A Quantum Theory, Oxford University Press, Oxford, 1990.
[19] N. Erdman, K.R. Poeppelmeier, M. Asta, O. Warschkow, D.E. Ellis, L.D. Marks, Nature 419 (2002) 55.
[20] O. Warschkow, M. Asta, N. Erdman, K.R. Poeppelmeier, D.E. Ellis, L.D. Marks, Surf. Sci. 573 (2004) 446.
[21] M.R. Castell, Surf. Sci. 505 (2002) 1.
[22] S.E. Stoltz, D.E. Ellis, M.J. Bedzyk, Surf. Sci. 630 (2014) 46–63.